Constructing an efficient conductive network with carbon-based additives in metal hydroxide electrode for high-performance hybrid supercapacitor

Guoshen Yang, Takahiro Takei, Yachao Zhu, Emad Iranmanesh, Binbin Liu, Zixuan Li, Jiawei Wang, Pritesh Hiralal, Gehan A.J. Amaratunga, Olivier Fontaine, et al.

Constructing an efficient conductive network with carbon-based additives in metal hydroxide electrode for high-performance hybrid supercapacitor

Guoshen Yang [a], Takahiro Takei [b], Yachao Zhu [c], Emad Iranmanesh [a], Binbin Liu [a], Zixuan Li [a], Jiawei Wang [a], Pritesh Hiralal [d], Gehan A.J. Amaratunga [e], Olivier Fontaine*[c, f, g], Hang Zhou*[a]

[a] *School of Electronic and Computer Engineering, Peking University Shenzhen Graduate School, Shenzhen, 518055, PR China*

[b] *Center for Crystal Science and Technology, University of Yamanashi, 7-32 Miyamae, Kofu, Yamanashi 400-8511, Japan*

[c] *ICGM, Universsité de Montpellier, CNRS, Montpellier, France.*

[d] *Zinergy Shenzhen Ltd., Gangzhilong Science Park, Longhua, Shenzhen, 518109, China*

[e] *Engineering Department, University of Cambridge, CB3 OFA, Cambridge, UK*

[f] *School of Energy Science and Engineering, Vidyasirimedhi Institute of Science and Technology (VISTEC), Rayong, 21210, Thailand.*

[g] *Institut Universitaire de France, 75005 Paris, France.*

Corresponding Authors:

* Hang Zhou: zhouh81@pkusz.edu.cn.

* Olivier Fontaine: olivier.fontaine@vistec.ac.th

ABSTRACT:

Progress toward the development of advanced supercapacitor technologies is closely associated with high-performance electrode materials. Carbon-based conductive additives modifying electrode material effectively improves the electronic conductivity and promotes the redox reaction. In this paper, we developed a highly effective binary conductive additive to modify cobalt aluminum layered double hydroxide (CoAl LDH) electrode with superior electrochemical performance, where the binary carbon species included carbon nanotubes (CNTs) and carbon nanohorns (CNHs). The as-constructed binary conductive additives CNTs/CNHs present a highly efficient electronic transmission network via a "line to the surface to point" mode. The as-prepared CoAl LDH@CNTs/CNHs electrode exhibits a significantly enhanced specific capacitance, superior rate capability, and stable cycle life. Based on analyzing and studying the characterizations and simulation, we reveal the electron transport mechanism and synergistic effects between CNTs/CNHs and CoAl LDH in a new perspective. The assembled hybrid supercapacitor device exhibits a high energy density (62.2 Wh/kg) and good cycling ability (79% retention after 5500 cycles). We believe that the binary conductive additives design strategy presented here is expected to apply to other energy storage such as batteries and pseudocapacitors.

KEYWORDS: binary conductive additives; electronic transmission network; CoAl layered double hydroxides; hybrid supercapacitor

1. Introduction

With the gradual exhaustion of fossil fuels and worsening global warming, we urgently need to develop energy storage devices to store electricity produced from renewable clean energy efficiently [1-2]. As a new generation of energy storage devices, supercapacitor (SC) has gained enormous attention due to its high-power density, high-rate performance, and long-life time [3-4]. Due to these advantages, SC is favorably applied in portable electronics and hybrid electric vehicles [5]. Nonetheless, the low energy density is hindering its future extensive application. A practical strategy is to fabricate a hybrid supercapacitor (HSC), which can have a higher energy density (than capacitor) with longer cycle life and higher power density (than battery). To produce a high-performance hybrid supercapacitor, innovative electrode materials such as transition metal hydroxide materials are critical [6]. Layered double hydroxides (LDHs) are ideal electrode materials due to their redox activity, structural controllability, and environmentally friendly nature [7-8]. However, the relatively low electronic conductivity, unsatisfactory rate capability, and poor cycling life of the LDHs essentially limit their practical applications. The literature on LDHs suggests that many attempts have been reported in recent articles, for instance, preparing nano-sized materials [9], trimetallic hydroxides [10-11], core/shell composite material [12-13], and combining with conductive carbon-based materials such as graphene [14] and carbon nanotubes [15]. Among various LDHs materials, CoAl LDH is prominent due to its excellent electrochemical properties and various production methods [16-19]. But it still suffers from the low rate and poor cycling stability. Generally, the electrode

comprises the conductive additive, electronic active material, and a polymeric binder. As a significant component of the electrode, the electronic conductive additive is critical to the electrochemical efficiency of HSC, especially in establishing a conductive percolation network to facilitate electron transport.

The most widely used conductive compounds are carbon-based materials. We can classify three types of carbon-based additives: zero-dimension (0D), one-dimension (1D) and two-dimension (2D) [20]. Like Super P (SP) as a typical 0D material with particle structure, carbon black has been commonly used as additive due to its good electronic conductivity and cost efficiency. However, it always suffers from heavy agglomeration, resulting in poor distribution on the electrode surface, which can cause grievous polarization and severe capacity loss of electrodes. Furthermore, the "point-to-point" contact mode between active materials particles (consider as 'point') and SP particles (consider as 'point') can result in relatively poor conductive efficiency [21]. Carbon nanotubes (CNTs), as a classic 1D material with a wire-like structure, are an advanced conductive additive, particularly in constructing a long-range electronic transmission network. Nevertheless, it is hard to distribute CNTs in the electrode homogenously, and the conductive efficiency of the "point-to-line" contact mode between active materials particles and CNTs (consider as 'line') is still unsatisfactory [22]. With the "plane to point" interaction mode between graphene (considers as 'plane') and active materials particles in the electrode, graphene, as a conventional 2D material with a sheet structure, may have a greater contact surface area than SP and CNTs [23].

Besides these common carbon materials, carbon nanohorns (CNHs), as a classic 0D material, have drawn increasing attention in recent years due to their unique Dahlia-like structure. Compared with the graphene and CNTs, CNHs display many good merits, such as easy preparation, large-scale, and low-cost [24]. Although CNHs have many promising applications [25-26], the exploration of CNHs as the conductive additive is still opening. The study about CNTs/CNHs as binary additives is vacant for the supercapacitor electrode. But carbon black/vapor-grown carbon fibers as a binary conductive additive have been reported to be an effective route to improve the capacitance performance of the $Li_{1.18}Co_{0.15}Ni_{0.15}Mn_{0.52}O_2$ electrodes for Li-ion batteries [27]. In this regard, CNTs/CNHs binary additives combining the merit of 0D CNH and 1D CNT should be an effective strategy, which can create an efficient electronic transmission network via a "line to the surface to point" mode (Surface specifically refers to the CoAl LDH nanosheets used in this study).

We report a binary conductive additives design strategy to prepare CoAl LDH@CNTs/CNHs electrode in this work. The as-constructed binary conductive additives CNTs/CNHs present a highly efficient electronic transmission network via a "line to the surface to point" mode. Switching to CNTs/CNHs from other carbon additives (SP, CNTs, CNHs and rGO), the new CoAl LDH electrode reveals a significantly enhanced electrochemical performance, which is attributed to the synergistic effects between the "line-to-surface" conductive mode (due to CNTs) with the long-range electron pathway and the "point-to-surface" conductive mode (due to CNHs) with the short-range electron pathway, respectively. The assembled CoAl

LDH@CNTs/CNHs//AC hybrid supercapacitor delivers a maximum energy density of 62.2 Wh/kg with a power density of 632.5 W/kg, specific capacitance can still maintain 79% after 5500 cycles.

2. Experimental section

2.1. Sample synthesis

2.1.1. Preparation of carbon materials

Briefly, a dc arc discharge in liquid nitrogen was generated between two graphite anode and cathode (purity > 99.999%), 6 and 24 mm in diameter. The discharge current was 600 A and the voltage was 20 V. After the discharge process, the collected CNHs were oxidized for 1 h at 550 °C in air. Super P was purchased from Switzerland TIMCAL Company. Hydroxylate multi-walled CNTs and rGO were purchased from China XFNANO Materials Tech Co., Ltd.

2.1.2. Preparation of the CoAl LDH composites electrode

The electrodes slurry was prepared by following steps. First, 85 wt% CoAl LDH (obtained from a hydrothermal method [9]), 5 wt% PTFE and 10 wt% conductive additives (10 wt% SP, 10 wt% CNHs, 10 wt% CNTs, 10 wt% rGO, 5 wt% SP+5 wt% CNTs, 5 wt% SP+5 wt% CNHs, 5 wt% rGO+5 wt% SP, 5 wt% rGO+5 wt% CNTs, 5 wt% rGO+5 wt% CNHs, 5 wt% CNTs+5 wt% CNHs) were mixed, and the mixture was dispersed in a certain of distilled water under magnetic stirring for 5h. Then, the slurry was uniformly coated on nickel current collector as the electrode with an area of 1×1 cm^2 and dried for 12h at 70 °C. The mass loading of active material was about 2 mg/cm^2.

2.2. Structural characterization and theoretical calculation

The molecular structure of the as-prepared sample was employed with Fourier transform infrared (FTIR) spectrometer (Bruker Vertex-70) and Raman spectrometer (LabRAM HR800, HORIBA JOBIN YVON S.A.S). The crystal phase of the samples was characterized by X-ray diffraction (XRD) (Bruker D8 Advance). The microstructural morphology characterization the samples was examined by scanning electron microscopy (SEM) (ZEISS SUPRA, Carl Zeiss) equipped with EDX analyzer. The morphological features of the samples were conducted on transmission electron microscopy (TEM) (JEM-3200FS, JEOL). The chemical composition of the samples was tested by X-ray photoelectron spectroscopy (XPS) (AXIS Ultra DLD, Kratos Analytical Ltd.). The computer simulations of the samples were calculated by use of the Vienna Ab Initio Simulation Package (VASP 5.3) [28-29]. In the simulations of the CNT, triple wall open-ended CNT was calculated with chiral vectors of (4, 4), (9, 9), and (14, 14). The simulation was carried out by PAW PBE potential. The structure was at first optimized and then the electronic structure was calculated. In the case of the simulation of LDH, we calculated CO_3^{2-} intercalated anion CoAl LDH. Actually, the existence of CO_3^{2-} makes the calculation difficult because of plural atoms in one CO_3^{2-} anion and its divalent nature. Within the interlayer space, the intercalated CO_3^{2-} state is unknown which CO_3^{2-} or HCO_3^-. Therefore, to simplify the calculation, CO_3^{2-} anion was set per one Al cation and the LDH was made negatively charged for compensation of charge. The compositional formula of the LDH can be shown as $Co_3Al(OH)_8(CO_3)$.

The simulation was carried out by PAW PBE potentials. The structure was optimized with a primitive cell and the electronic structure was simulated.

2.3. Electrochemical measurement

All electrochemical tests were examined by an electrochemical workstation (CHI660E, Shanghai CH Instrument Co., Ltd.) within a three-electrode cell configuration consisting of working electrode (Ni foam/sample), platinum counter electrode, Hg/HgO reference electrode, and 6 M KOH electrolyte, respectively. The electrochemical impedance spectroscopy (EIS) spectra were collected in the frequency range of 0.01-100 kHz with an amplitude of 5 mV.

2.4. Assembly of aqueous hybris supercapacitor devices

For full-cell (HSC) fabrication, the CoAl LDH was served as the cathode, and activated carbon (AC) was used as the anode, whereas the 50 μm thick fiberglass as the separator and 6 M KOH as the electrolyte into a test fixture. The AC electrode was prepared with a similar routine by mixing 85 wt% AC, 5 wt% PTFE and 10 wt% acetylene black. To meet the demand of $Q^+ = Q^-$, below formula determined the weight ratio between the CoAl LDH and AC:

$$\frac{m_+}{m_-} = \frac{C_- \cdot \Delta E_-}{C_+ \cdot \Delta E_+}$$

where m (g), C (F/g), ΔE (V) were the mass of active material, specific capacitance, and potential window of the CoAl LDH and AC electrode, respectively. The electrochemical tests of the assembled HSC device were performed on the same electrochemical device.

3. Results and discussion

3.1. Structural study

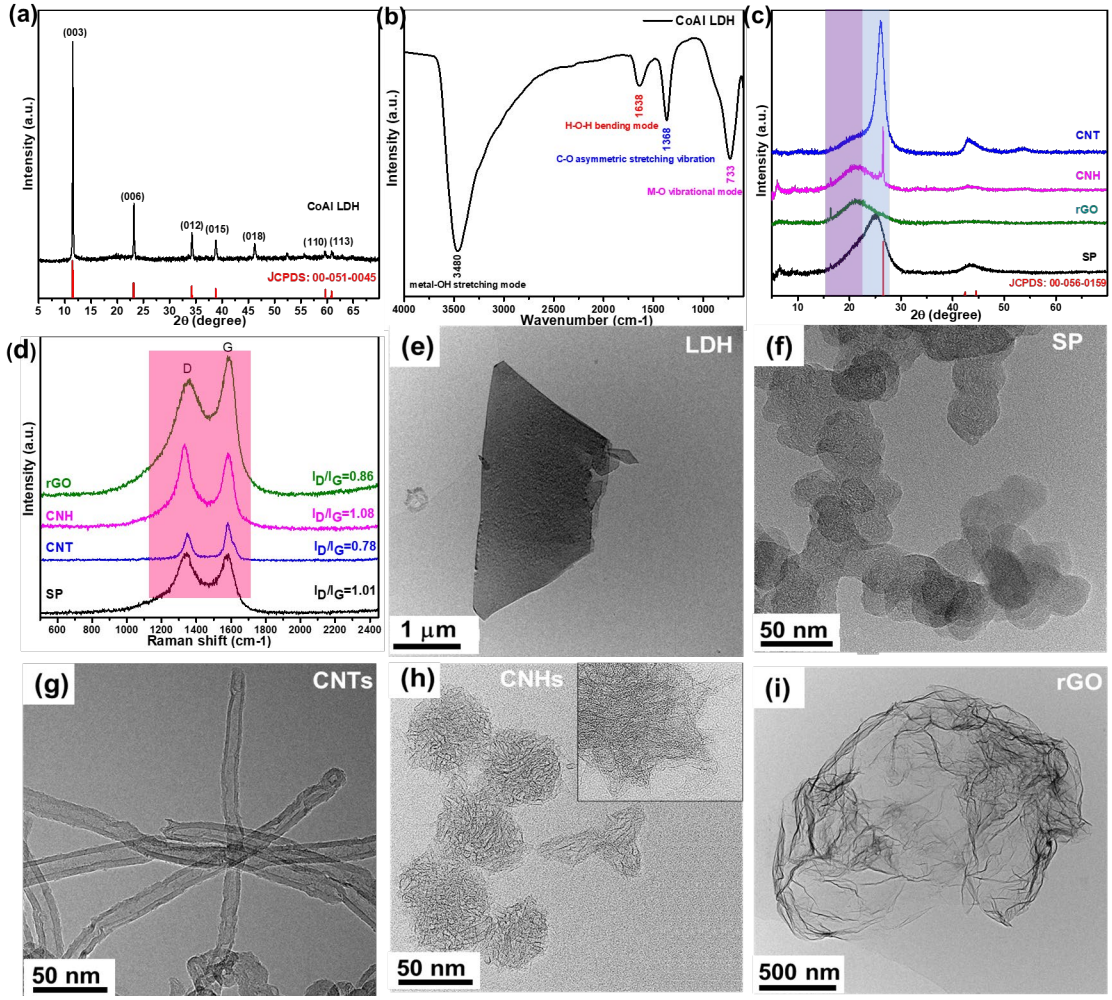

Fig. 1. (a, b) XRD patterns and FTIR spectra of CoAl LDH. (c, d) XRD and Raman spectra of SP, CNTs, CNHs, and rGO. (e-i) TEM images of CoAl LDH, SP, CNTs, CNHs, and rGO. (A color version of this figure can be viewed online.)

XRD and FTIR were used to characterize the structure of as-prepared CoAl LDH and carbon-based conductive additives. The XRD patterns of CoAl LDH powder (Fig. 1a) are consistent with that of the desired CoAl LDH phase (JCPDS: 00-051-0045) [30]. The broad absorption band in Fig. 1b around 3480 cm^{-1} are attributed to the metal-OH stretching mode and H-bonded interlayer H_2O surrounding the interlayer anion, and the

corresponding H-O-H bending mode of interlayer H_2O appears at about 1638 cm^{-1}. The intense peak at about 1368 cm^{-1} is attributed to the C-O bond's asymmetric stretching vibration caused by the interlayer of CO_3^{2-} in CoAl LDH. The lower wavenumber absorption band at around 733 cm^{-1} belongs to the M-O, O-M-O, and M-O-M involved vibrational modes of LDHs [31]. The XRD patterns and FTIR spectra together prove the successful preparation of CoAl LDH nanomaterials. The XRD patterns of SP, CNTs, CNHs, and rGO are shown in Fig. 1c. The diffraction peak of SP and CNTs at around 26° corresponds to the (002) characteristic reflection of graphite. SP, on the other hand, has a larger (002) peak than CNTs, indicating its amorphous existence and smaller particle size [27]. In contrast, the narrower (002) peak of CNTs indicates its higher crystallinity. The rGO diffraction peak at approximately 22° correlates to the graphite (002) reflection, meaning that graphene oxides are efficiently reduced. The as-prepared CNTs showed sharp diffraction at around 22°, assigned to the (002) peak of graphene-like structure [32]. Raman spectra of carbon additives are depicted in Fig. 1d, where two characteristic peaks at around 1350 cm^{-1} and 1590 cm^{-1} are the typical D and G bands, respectively. The intensity ratio of I_D/I_G bands reflects the concentration of defects for carbon-based materials [33]. It is found that the CNHs have a higher I_D/I_G value (1.08) than SP (1.01), CNTs (0.78), and rGO (0.88), suggesting that it formed more defects in CNHs. The obtained result is also consistent with previously reported data [24].

SEM and TEM examined the morphological and structural features of the as-synthesized CoAl LDH and carbon-based conductive additives. The CoAl LDH bulk

shows a typical flower-like morphology with many aggregated nanosheets (Fig. S1a). The resultant nanoparticles are hexagonal-shape nanosheets structures with a lateral size of *ca.* 1.5-4 μm (Fig. 1e). In addition to the difference in crystallinity, SP, CNTs, CNHs, and rGO also displayed noticeable differences in morphological features. The SP displays the agglomerated structure (Fig. S1b), and the spherical nanoparticles are observed with the size from 25 to 50 nm (Fig. 1f). The CNTs presents fiber-like morphology with bend and entangled cylindrical tubes (Fig. S1c). It shows a hollow structure with outer diameters of *ca.* 20-30 nm (Fig. 1g). The CNHs aggregate into ball-shape clusters (Fig. S1d), and they exhibit a typical dahlia-like structure with the protruding horn structure with a length of *ca.* 40 nm (Fig. 1h). The rGO displays sheet-like morphology and the wrinkled sheet structure with large-scale sizes ranging from 4 to 6 μm (Fig. S1e and Fig. 1i), which are the typical structural features rGO [34]. Compared to other carbon materials, rGO shows the largest specific surface area (Fig. S2).

XPS and EDX further characterized the chemical composition and elemental distribution of the CoAl LDH. As shown in Fig. S3a, the full XPS spectrum of as-synthesized sample indicates the existence of elements of Co, Al, C, and O, further proving the existence of stacked CO_3^{2-} intercalated anion in CoAl LDH, which is accord with the above FTIR analysis. Likewise, as shown in Fig. S3b-3e, the Co 2p, Al 2p, C 1s and O 1s spectrum are in accord with previously reported results (see Supporting Information Fig. S3 for details) [10, 35]. EDX mapping analysis (Fig. S3f-3h) exhibits a homogeneous distribution of the elements (Co, Al, C, O) in the CoAl LDH.

3.2. Electrochemical measurements

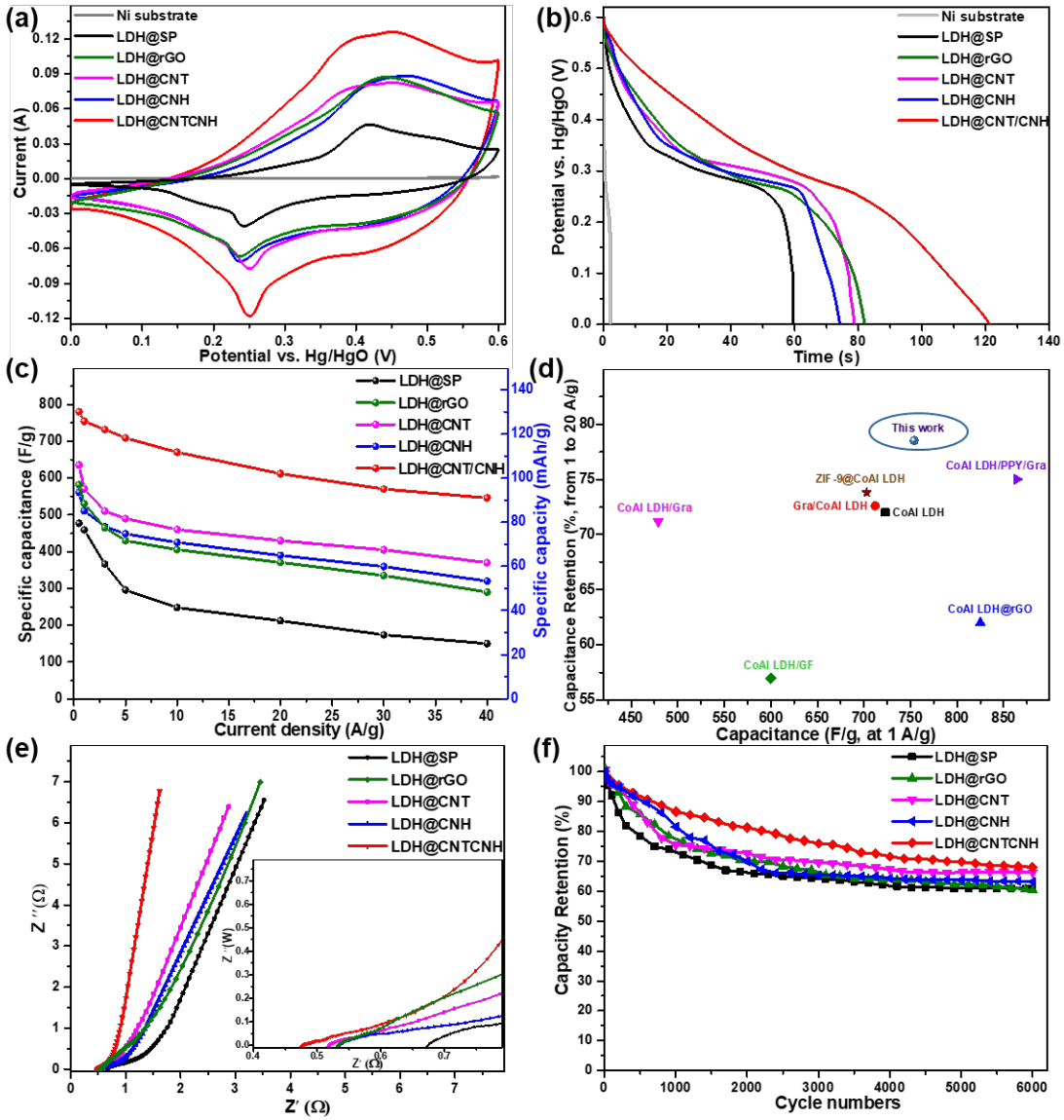

Fig. 2. (a, b) CV and GCD curves of Ni substrate and as-prepared CoAl LDH-based electrodes (scan rate 20 mV/s and current density 3 A/g). (c) Specific capacitance and specific capacity values of as-prepared CoAl LDH-based electrodes at versus current density. (d) Balance relationship between capacitance retention and capacitance for different CoAl LDH-based electrode. (e) Nyquist plots and (f) Cycling performance of the as-prepared CoAl LDH-based electrodes. (A color version of this figure can be viewed online.)

The electrochemical measurements for the as-synthesized electrodes were examined by a three-electrode system. Fig. 2a displays the CV curves of the Ni current

collector and as-prepared electrodes. The results show that the Ni current collector contributes to negligible capacitance. In LDH-based electrodes, one pair of well-separated cathodic/anodic peaks is observed in all CV curves, deriving from the quasi-reversible Faradic redox reaction (1) [31].

$$Co(OH)_2 + OH^- \leftrightarrow CoOOH + H_2O + e^- \quad (1)$$

More precisely, unlike the standard pseudocapacitive behavior, the CV curves of CoAl LDH-based electrodes show the battery-like behavior [36]. The appropriate metrics for CoAl LDH is to use the concept of charge capacity (mAh/g) and capacitance (F/g) together [6]. Notably, the CoAl LDH@CNTs/CNHs has the largest CV enclosed area, indicating that the CNTs/CNHs binary conductive additive for CoAl LDH electrode endue an enhanced specific capacitance. A similar tendency is also observed in GCD curves (Fig. 2b). The CoAl LDH@CNTs/CNHs electrode displays the longest discharge time compared to other electrodes. As a result, it shows the highest specific capacitance of 754 F/g (125.7 mAh/g) at 1 A/g. More significantly, the distinct potential plateau in GCD curves implies the related faradaic reaction process, which is also consistent with the analysis result of CVs. One purpose of this study was to evaluate the rate capability of the CoAl LDH@CNTs/CNHs electrode, the CV and GCD measurements were carried out. Fig. S4a shows the CV curves of CoAl LDH@CNTs/CNHs electrode at various sweep rates. It is found that the cathodic and anodic peaks shift toward the negative and positive potentials without any apparent variation even at a high scan rate, revealing the excellent reversibility of faradaic

reactions. The charge storage kinetics is evaluated by analyzing the correlation between cathodic/anodic peak current (i, A) and scan rate (v, mV/s) (equation 2) [37-39]:

$$i = av^b \quad (2)$$

where a and b are constants. Usually, b=0.5 indicates that the electrode reaction is a diffusion-controlled process, while b=1.0 indicates that the electrode reaction is a surface-controlled process. The value of b can be obtained by linear fit calculation of $\log_{(i)}$ against $\log_{(v)}$. For the CoAl LDH@CNTs/CNHs electrode, the b values of the anodic and cathodic peaks are 0.78, 0.81, respectively, indicating that the charge storage process combines a diffusion-controlled along with increase contribution (Fig. S4b). The diffusion/capacitive-controlled contributions of CoAl LDH@CNTCNH is also further calculated [40-41] (see Supporting Information Fig. S4 for details). Fig. S4c shows a typical CV curve at 5 mV/s, revealing 71.4% capacitive contribution of the total capacitance. With the increase of scan rate, the capacitive contribution gradually increases to 95% at 50 mV/s, implying the capacitive-dominant charge storage (Fig. S4d).

Fig. S4e displays the GCD curves of the as-synthesized CoAl LDH@CNTs/CNHs electrode at various current densities. The profoundly nonlinear and voltage plateau clarifies the battery-type characteristic of CoAl LDH@CNTs/CNHs. By calculation, the specific capacitance of CoAl LDH@SP, CoAl LDH@rGO, CoAl LDH@CNTs, CoAl LDH@CNHs, and CoAl LDH@CNTs/CNHs are 477, 581, 632, 560, and 780 F/g at 0.5 A/g and the specific capacitance retentions of them are 31%, 50%, 58%, 56%, and 70% from 0.5 to 40 A/g, respectively (Fig. 2c). The specific capacitance and rate capability of the CoAl LDH@CNTs/CNHs electrode are among the best

supercapacitive performance compared with those of CoAl LDH with individual carbon-based conductive additives. In order to further study the influence of binary conductive additives on CoAl LDH electrode, we further performed galvanostatic charge-discharge measurements of a series of CoAl LDH cathodes with different binary carbon-based additives. The rate performances of the CoAl LDH electrodes with different binary carbon-based additives are compared in the same ratio in Fig. S5. Fig. S6. shows the specific capacitance values of as-prepared CoAl LDH electrodes with different carbon-based additives. Compared with single conductive agent, CoAl LDH electrodes with binary conductive agents usually exhibited higher capacitance. A detailed comparison of as-prepared CoAl LDH electrodes with different carbon-based additives is summarized in Table S1. Compared with single conductive agent, CoAl LDH electrodes with binary conductive agents usually exhibited higher capacitance and capacitance retention, but they are closely related to the contact mode between active materials and conductive additives. Among them, the as-constructed binary conductive additives rGO/CNT, rGO/CNH and CNT/CNH present a highly efficient electronic transmission network via “line to surface to plane” mode, “point to surface to point” and “line to surface to point” modes, respectively. The as-prepared CoAl LDH@CNTs/CNHs electrode exhibits a significantly enhanced specific capacitance and rate performance. Furthermore, considering the high cost of rGO, CNTs/CNHs as binary additives is the promising methodology. Moreover, the superior rate performance of CoAl LDH@CNTs/CNHs in Fig. 2d can also surpass many previously

reported CoAl LDH-based electrode materials (see Supporting Information Table S2 for details).

EIS measurements were performed to evaluate the ion diffusion and electron transfer in the electrolyte/electrode system. Usually, the intersecting point with the real axis represents the equivalent series resistance (R_s). In contrast, the diameter of the approximate semi-circle represents charge transfer resistance (R_{ct}), and the straight slope represents the Warburg impedance (Z_w) related to the diffusion resistance of the OH^- electrolyte ions in the electrode materials. The Rs values of CoAl LDH@SP, CoAl LDH@rGO, CoAl LDH@CNTs, CoAl LDH@CNHs and CoAl LDH@CNTs/CNHs in Fig. 2e are 0.68, 0.53, 0.52, 0.52, and 0.48 Ω, respectively, indicating the most negligible electrode resistance with the addition of CNTs/CHNs binary additives. Compared to other electrodes, reduced diameter of the semicircle and increased slope of the straight line are observed for CoAl LDH@CNTs/CNHs. It proves that the existence of binary additives reduces the charge transfer in CoAl LDH@CNTs/CNHs electrode, suggesting the improved charge transfer kinetics over the redox process and lower ion diffusion resistance. Additionally, the slope of the CoAl LDH@CNTs/CNHs electrode is significantly greater than 45°, revealing a mechanism that combines diffusion and surface processes. The above results show the significant role of CNTs/CNHs binary conductive additives, which can offer a highway for electron/ion transport and facilitate electrochemical reaction kinetics. In addition, the long cycling measurement of the as-prepared electrodes was carried out at 5 A/g within the potential window of 0-0.6 V. As cycle number increases, the CoAl LDH@CNTs/CNHs electrode

experiences a slower deterioration process in comparison with others, resulting in overall high capacitance retention of 81.7% after 6000 cycles (Fig. 2f). As shown in Fig. S7, after 6000 cycles, the CoAl LDH nanosheets and the as-constructed binary conductive additives CNTs/CNHs can be clearly observed, which indicate its good cycle life.

3.3. Mechanism of CoAl LDH@CNTs/CNHs achieving enhanced electrochemical performance

Based on the CV and GCD results, CoAl LDH electrode with CNTs/CNHs binary conductive achieved enhanced specific capacitance, superior rate capability, and long-term cycle life compared with those of CoAl LDH with individual carbon-based conductive additives. Based on the EIS results, CoAl LDH@CNTs/CNHs electrode displayed lower R_s and R_{ct} amount among all electrodes, indicating that the CNTs/CNHs binary conductive additive has better electrical conductivity. Nevertheless, a fundamental understanding of the synergistic effect of each component about electronic transmission regarding CNTs/CNHs and CoAl LDH is a key issue to understand performances. As reported by previous study [42-44], the improved electrochemical performance of carbon-based conductive additive modifying LDH electrode material was easy to attribute the high conductivity of the conductive additive. However, a fundamental understanding of the synergistic effect of each component about electronic transmission regarding CNTs/CNHs and CoAl LDH is a key issue to understand performances. However, nothing is understood regarding the further investigation of the active material's synergistic effects with the conductive additive. It

has a great significance for us to understand how redox reaction occurred in electrode materials. Thus, it is profoundly significant to figure out the mechanism in the electrode with conductive additive.

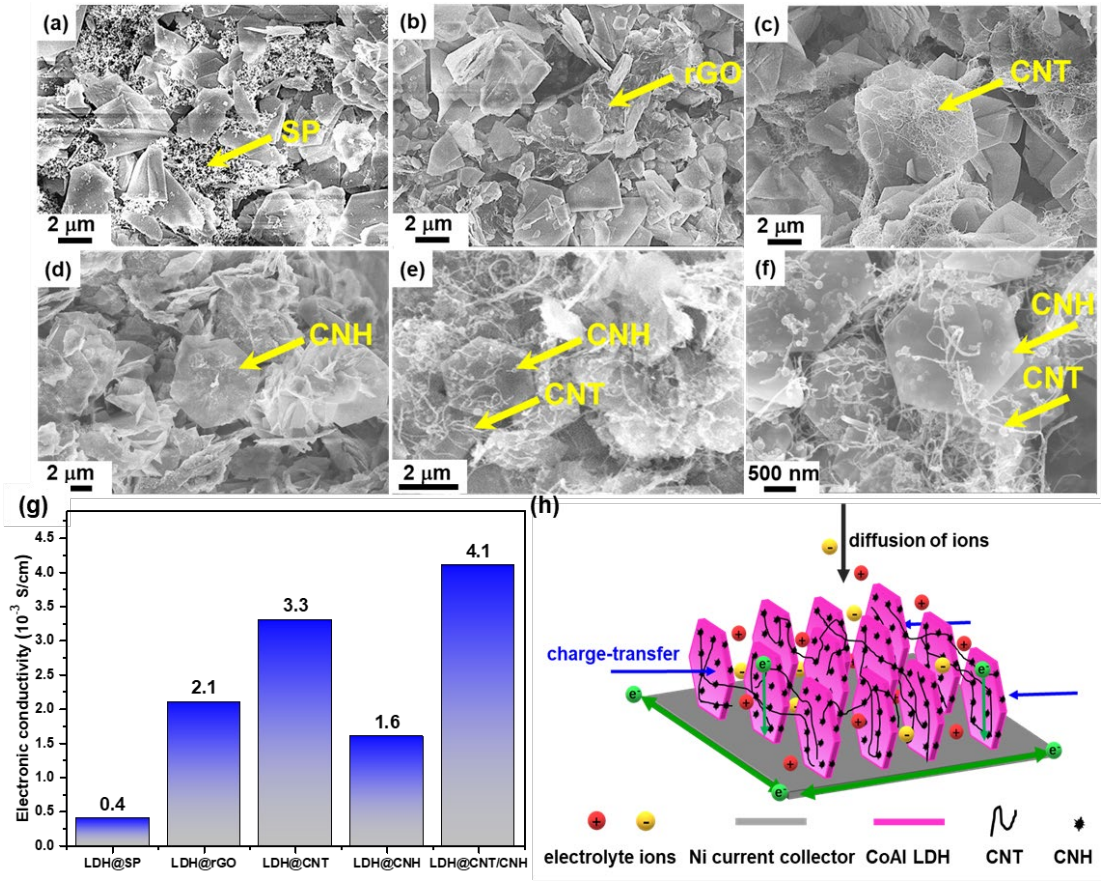

Fig. 3. Surface SEM morphology of (a) LDH@SP, (b) LDH@rGO, (c) LDH@CNTs, (d) LDH@CNHs, and (e, f) LDH@CNTs/CNHs electrodes. (g) The electronic conductivity of the CoAl LDH electrodes prepared by different conductive additives. (h) Schematic illustration of electrolyte ions diffusion paths in CoAl LDH with CNTs/CNHs as the conductive additive. (A color version of this figure can be viewed online.)

We first observed the surface morphology of the as-prepared electrode. Fig. 3a-3f displays the surface morphology of the CoAl LDH electrode with different conductive additives. As presented in Fig. 3a, the smaller SP particles heavily agglomerate together.

They are easily trapped in the inter voids between the more extensive CoAl LDH nanoplates, forming a “point to surface” conductive network. As a result, the isolated CoAl LDH nanoplates have not been well connected by the SP, and the conductive paths in the CoAl LDH electrode are interrupted. As presented in Fig. 3b, the CoAl LDH nanoplates are covered by rGO, forming a “plane to surface” effective electron conductive network. However, as mentioned in Fig. 1f and Fig. 1n, the lateral size of rGO was larger than CoAl LDH, which may cause the electrolyte ions diffusion hindered to some extent. In Fig. 3c, the long wire-like CNTs can connect with multiple CoAl LDH nanoplates to construct a long-range conductive network, forming a “line to surface” conductive network. However, wire-like CNTs are not homogenously distributed in bulk, which causes poor surface coverage on the CoAl LDH nanoplates. In Fig. 3d, the smaller CNHs are uniformly distributed on the surface of the CoAl LDH nanoplates, forming a “point to surface” conductive network. More important, in Fig. 3e-3f, the CoAl LDH nanoplates are inserted in a conductive network consisting of CNHs and CNTs, which provides a highly efficient electronic transmission network via a “line to surface to point” mode. The fibrous CNTs play an essential role in bridging the isolated CoAl LDH nanoplates. CNHs have the ability to fill in/on the surface and interspace of the CoAl LDH nanoplates, resulting in the formation of stronger physical connections between the CoAl LDH and the conductive network linked by CNTs. This kind of binary conductive additive constructs an interactive network, consequently more efficient electronic transmission. The electronic conductivity is measured to reflect the connection of the network. In Fig. 3g, the CoAl LDH@CNTs/CNHs

electrode exhibits the highest electronic conductivity of 4.1×10^{-3} S/cm compared with those of CoAl LDH with individual carbon-based conductive additives. It powerfully demonstrates that CNTs/CNHs binary additive can build a more efficient conductive network than a single conductive additive.

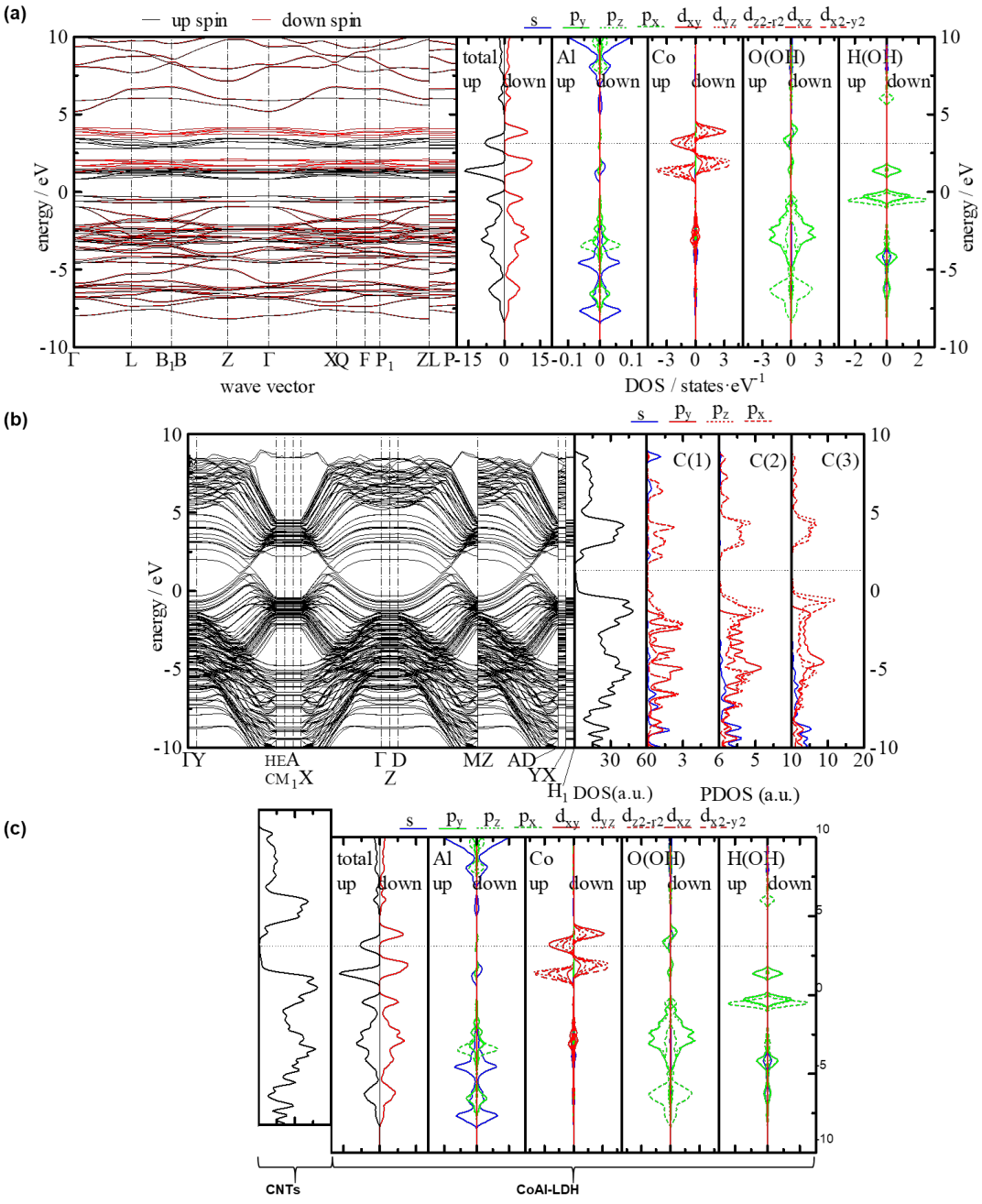

Fig. 4. (a, b) Band dispersion and DOS curves of CoAl LDH and CNTs. (c) DOS curves of the composite of CoAl LDH and CNTs. (A color version of this figure can be viewed online.)

Up to this point, a comprehensive understanding of the underlying electronic transmission mechanisms with respect for conductive additives, and the active material is still missing. Herein, a novel viewpoint from the perspective of the band structure was proposed. For the band dispersion and density of states (DOS) curves of CoAl LDH, the Fermi level was shown by the thin dotted line (Fig. 4a). These curves show that the Fermi level is at 0 V. From the band dispersion curve, the Fermi level was slightly below the conduction band minimum, which was composed of down spin. Due to no recognized band gap, the state of CoAl LDH seems to have metallic properties. However, the band dispersion curves near the Fermi level have a huge curvature radius, which means a very heavy effective mass of the electron. Therefore, the electronic conductivity should be very low in the CoAl LDH, consistent with our previous reports [9]. Fig. 4b shows the band dispersion and DOS curves of CNTs. From the DOS curves, the bandgap seems to exist. However, the band dispersion diagram indicates no bandgaps in the CNTs. In addition, the radius of curvature for the band dispersion curves is much smaller than that of the CoAl LDH.

Therefore, the electron conductivity should be very high, which can help electron displacement and redox reaction of the CoAl LDH. For the composite structure of the CoAl LDH and CNTs, the electronic band will be shifted to coincide with each Fermi level as the left-hand side figure (Fig. 4c). In the case of such a hybrid, we have to estimate the junction between two materials. Generally, the band structure should be bent with the coincidence of the fermi levels of both materials like Schottky conduction. The Schottky barrier generally shows the rectification in which the electron can move

in only one direction from the semiconductor to the metallic phase. The Schottky barrier can be estimated as the difference between the CBM of the semiconductor and the Fermi level of the metallic phase. For our CoAl LDH, Co^{2+} shows a low spin state and the energy gap between E_g and t_{2g} is around 2 eV. The Fermi level of the LDH is just in the e_g orbital and consequently has no energy gap like a general semiconductor. From these considerations, the contact of the CNT and LDH results in only band bending and no Schottky barrier. Consequently, the contact of the CNT and LDH may make fair bidirectional conductivity. As shown in Fig. 4c, redox reaction between Co^{2+} and Co^{3+} should occur at nearby the Fermi level. The Co^{2+} cation has seven d-electrons stored for 6 at the t_{2g} and for 1 at the e_g levels. The six electrons at t_{2g} can be distinguished to 3 with up spin and 3 with down spin. The one electron in the e_g level should be up spin, and it should be released and come back by redox reaction via CNTs to the substrate metal. This electronic transmission mechanism is also suitable for CNHs. Consequently, such a composite structure is necessary for an efficient redox reaction to improve its electrochemical performance.

In the light of the above results, the highlighted electrochemical performance of CoAl LDH@CNTs/CNHs electrode can attribute to the below points: (1) The CoAl LDH nanoplates were uniformly coated on/in the porous nickel foam current collector, resulting in low contact resistance. The porous structures of Ni foam can facilitate the rapid transfer of electrolyte ions. (2) Binary conductive additives CNTs/CNHs were used to construct a highly efficient electronic transmission network via a “line to surface to point” mode (Fig. 3h). The CNTs/CNHs were coated on the surface of the CoAl LDH

nanoplates as well as cover the void spaces. They could build an interconnected bridge between the isolated CoAl LDH nanoplates by the binder to facilitate electron transport. The short-range electronic transmission pathway can be effectively constructed using circular CNHs particles of small scale, whereas the long-range electronic transmission pathway can be successfully constructed using wire-like CNTs. (3) As mentioned above, the particle of CoAl LDH is greater than the additives (both SP, CNHs and CNTs). Unlike rGO, when CNTs/CNHs were used as a conductive additive, the OH^- ion diffusion pathway will not be markedly obstructed, due to many exposed surfaces still exist. Moreover, hydroxylated CNTs/CNHs can efficiently adsorb electrolyte on the surface of the CoAl LDH nanoplates, reducing the ion transport path. Thus, the CoAl LDH@CNTs/CNHs electrode exhibits excellent electrochemical performance.

3.4 Hybrid supercapacitor device

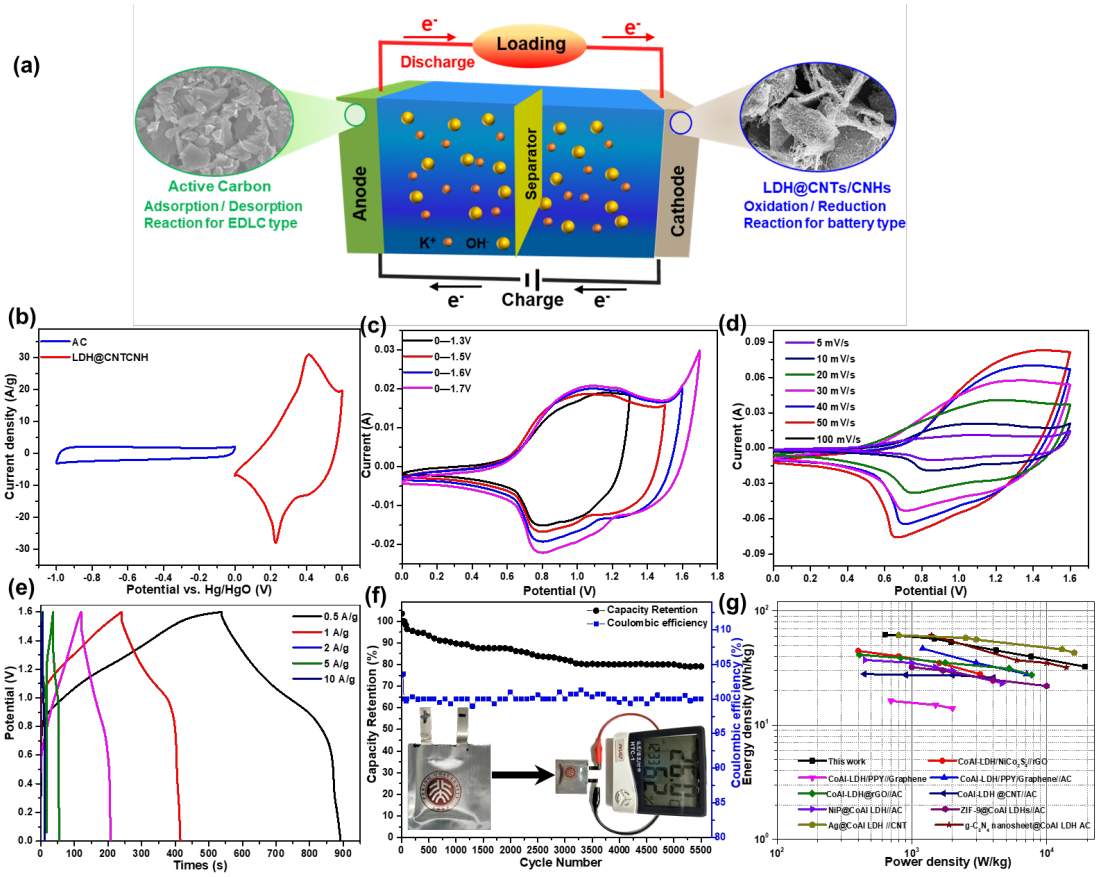

Fig. 5. (a) Schematic illustration of the CoAl LDH@CNTs/CNHs//AC HSC device. (b) CV curves of CoAl LDH@CNTs/CNHs and AC electrodes at 5 mV/s in three-electrode system, respectively. (c) CV curves of the HSC device in various voltages at 20 mV/s. (d) CV curves of the HSC device at different scan rates. (e) GCD curves of the HSC device at various current densities. (f) Cycling performance at the current density of 5 A/g and the devices in series can lighten up an electric desktop clock (inset). (g) Ragone plots of HSC device [43, 45-51]. (A color version of this figure can be viewed online.)

To order to validate the practical applications of the as-prepared electrodes, we constructed an aqueous CoAl LDH@CNTs/CNHs HSC, as shown in schematic diagram of HSC in Fig. 5a. Due to the combination of battery-type CoAl LDH anode and EDLC-type AC cathode, the assembled HSC can store charge through reversible faradaic redox reaction onto cathode and electrolyte anion adsorption/desorption onto

AC anode. Thus, significantly improved energy and power densities may be achieved for this device. The appropriate potential ranges of HSC were investigated by the CV curves of CoAl LDH@CNTs/CNHs and AC. The AC and CoAl LDH@CNTs/CNHs can well work in the potential range of -1-0 V and 0-0.6 V, respectively (Fig. 5b). The electrochemical performance of the AC negative electrode is also displayed in Fig. S8. In Fig. S8a, even at a high scan of 50 mV/s, the anodic/cathodic peak current of the AC electrode is also highly symmetric, indicating excellent reversibility. The capacitance retention of AC is 67% from 0.5 to 40 A/g, indicating its superior rate performance (Fig. S8b). As shown in Fig. 5c, to better optimize the voltage window of assembled HSC, a series of CV measurements at varying potential range starting from 0 to 1.7 V were carried out. In detail, the CV curve within 1.6 V without any noticeable distortion; however, an apparent polarization phenomenon was observed with further expansion of window voltage to be 1.7 V, which is associated with oxygen evolution reaction on the cathode surface. Consequently, the suitable potential window of HSC was 0 to 1.6 V. As shown in Fig. 5d, with increasing the scan rate, the CV shape preserved well at a high rate, which implied its good rate performance. Fig. 5e shows the GCD curves at various current densities. The capacitances of CoAl LDH@CNTs/CNHs were calculated as 175, 161, 142, 112, and 89 F/g at 0.5, 1, 2, 5, and 10 A/g, respectively. The capacity retention of HSC is 51% from 0.5 to 10 A/g, indicating its good charge storage ability. The cycling stability of HSC device was tested by charge-discharge process at 5 A/g. As shown in Fig 5f, after 5500 charge-discharge cycles, the HSC device maintains 79% retention of the initial capacitance. To verify its practical

application, the assembled HSC was used to light an electric desktop clock after being charged to 1.6 V (inset of Fig. 5f), indicating the high-power output of CoAl LDH@CNTs/CNHs//AC device.

To assess the HSC device's output in terms of energy and power density, the Ragone plot of CoAl LDH@CNTs/CNHs//AC is obtained, as shown in Fig. 5g. When the current densities are 0.5, 1, 2, 5, and 10 A/g, the corresponding energy densities are 62.2, 57.2, 50.5, 39.8, and 22.8 Wh/kg, and the power densities are 632.5, 1465.7, 1954, 7680, and 19221.5 W/kg, respectively. Compared to traditional supercapacitors, our assembled HSC device displays an apparent higher energy density than reported CoAl LDH-based supercapacitor devices without compromising the power density [43,45-50].

4. Conclusions

In this work, the CoAl layered double hydroxide (LDH) nanomaterials were successfully synthesized through a facile hydrothermal route. A binary CNTs/CNHs additive for CoAl LDH battery-type electrode was elaborately designed. The morphology and electrochemical performances of the CoAl LDH with a single conductive agent (0D SP, 1D CNTs, 0D CNHs, and 2D rGO) were also conducted for comparison. The prepared CoAl LDH@CNTs/CNHs displays a dramatically improved specific capacitance (754 F/g or 125.7 mAh/g at 1 A/g), excellent rate capability (78.5% capacitance retention at 20 A/g), and superior cycling stability (81.7% retention after 6000 cycles). The electrode's superior electrochemical properties are due to the intricately built binary conductive additives and the synergistic impact of CNTs/CNHs

and CoAl LDH. The possible mechanism of the electron transport mechanism and synergistic effects between CNTs/CNHs and CoAl LDH is also proposed in a new perspective. The assembled CoAl LDH@CNTs/CNHs//AC HSC exhibits the maximum energy density of 62.2 Wh/kg at 632.5 W/kg. Its specific capacitance can maintain 79% after 5500 cycles, suggesting great potential applications in energy storage systems. Our hybrid supercapacitor device could bridge the energy density gap between battery and supercapacitor for energy storage. The binary conductive additives design strategy presented here can be extended to construct other metal hydroxides/oxides electrodes. It could apply to other energy storage such as batteries and pseudocapacitors.

CRediT authorship contribution statement

Guoshen Yang: Conceptualization, Investigation, Data curation, Writing-original draft. **Takahiro Takei:** Formal analysis, VASP calculation. **Yachao Zhu:** Formal analysis, Investigation. **Emad Iranmanesh:** Formal analysis. **Binbin Liu:** Formal analysis**. Zixuan Li**: Formal analysis. **Jiawei Wang:** Formal analysis. **Pritesh Hiralal:** Investigation. **Gehan A.J. Amaratunga:** Investigation. **Olivier Fontaine:** Visualization, Validation, Writing - review & editing. **Hang Zhou:** Funding acquisition, Resources, Supervision, Visualization, Validation, Writing - review & editing.

Declaration of competing interest

The authors declare that they have no known competing financial interests or personal relationships that could have appeared to influence

Acknowledgments

This work is supported by Shenzhen Science and Technology Innovation Committee (No. GJHZ20190820091203667, No. JCYJ20190806145609284), Guangdong Basic and Applied Basic Research Foundation (2020A1515010716), and the Guangdong Introducing Innovative and Entrepreneurial Teams Program (2019ZT08Z656). P. Hiralal would like to acknowledge Shenzhen Science and Technology Program (KQTD20190929172522248). Technical support from Tsinghua Shenzhen International Graduate School Materials and Devices Testing Center is gratefully acknowledged. O.F also acknowledges the Institut Universitaire de France for the support.

REFERENCES

[1] G. Wang, L. Zhang, J. Zhang, A review of electrode materials for electrochemical supercapacitors, Chem. Soc. Rev. 41 (2012) 797-828.

[2] M. Inagaki, H. Konno, O. Tanaike, Carbon materials for electrochemical capacitors, J. Power Sources 195 (2010) 7880-7903.

[3] P. Simon, Y. Gogotsi, B. Dunn, Where Do Batteries End and Supercapacitors Begin?, Science 343 (2014) 1210-1211.

[4] L. F. Chen, Y. Lu, L. Yu, X. W. Lou, Designed formation of hollow particle-based nitrogen-doped carbon nanofibers for high-performance supercapacitors, Energy Environ. Sci. 10 (2017) 1777-1783.

[5] Y. Da, J. Liu, L. Zhou, X. Zhu, X. Chen, L. Fu, Engineering 2D Architectures toward High-Performance Micro-Supercapacitors, Adv. Mater. 31 (2019) 1802793.

[6] J. M. Gonçalves, M. I. da Silva, H. E. Toma, L. Angnes, P. R. Martins, K. Araki, Trimetallic oxides/hydroxides as hybrid supercapacitor electrode materials: a review, J. Mater. Chem. A 8 (2020) 10534-10570.

[7] J. Huang, T. Lei, X. Wei, X. Liu, T. Liu, D. Cao, J. Yin, G. Wang, Effect of Al-doped β-$Ni(OH)_2$ nanosheets on electrochemical behaviors for high performance supercapacitor application, J. Power Sources 232(2013) 370-375.

[8] K. H. Goh, T. T. Lim, Z. Dong, Application of layered double hydroxides for removal of oxyanions: a review, Water Res. 42 (2008) 1343-1368.

[9] G. Yang, T. Takei, S. Yanagida, N. Kumada, Enhanced supercapacitor performance based on CoAl layered double hydroxide-polyaniline hybrid electrodes manufactured using hydrothermal-electrodeposition technology, Molecules 24 (2019) 976.

[10] Y. Xiao, D. Su, X. Wang, S. Wu, L. Zhou, Z. Sun, Z. Wang, S. Fang, F. Li, Ultrahigh energy density and stable supercapacitor with 2D NiCoAl Layered double hydroxide, Electrochim. Acta 253 (2017) 324-332.

[11] S. Zhang, J. Liu, P. Huang, H. Wang, C. Cao, W. Song, Carbonaceous aerogel and CoNiAl-LDH@CA nanocomposites derived from biomass for high performance pseudo-supercapacitor, Sci. Bull. 62 (2017) 841-845.

[12] W. Hong, J. Wang, L. Niu, J. Sun, P. Gong, S. Yang, Controllable synthesis of CoAl LDH@ $Ni(OH)_2$ nanosheet arrays as binder-free electrode for supercapacitor applications, J. Alloys Compd. 608 (2014) 297-303.

[13] J. Han, Y. Dou, J. Zhao, M. Wei, D. G. Evans, X. Duan, Flexible CoAl LDH@ PEDOT core/shell nanoplatelet array for high-performance energy storage, Small 9 (2013) 98-106.

[14] Z. Wang, X. Zhang, J. Wang, L. Zou, Z. Liu, Z. Hao, Preparation and capacitance properties of graphene/NiAl layered double-hydroxide nanocomposite, J. Colloid Interface Sci. 396 (2013) 251-257.

[15] M. Li, J. E. Zhu, L. Zhang, X. Chen, H. Zhang, F. Zhang, S. Xu, D. G. Evans, Facile synthesis of NiAl-layered double hydroxide/graphene hybrid with enhanced electrochemical properties for detection of dopamine, Nanoscale 3 (2011) 4240-4246.

[16] Z. P. Diao, Y. X. Zhang, X. D. Hao, Z. Q. Wen, Facile synthesis of CoAl-LDH/MnO_2 hierarchical nanocomposites for high-performance supercapacitors, Ceram. Int. 40 (2014) 2115-2120.

[17] E. Musella, I. Gualandi, E. Scavetta, A. Rivalta, E. Venuti, M. Christian, V. Morandi, A. Mullaliu, M. Giorgetti, D. Tonelli, Newly developed electrochemical synthesis of Co-based layered double hydroxides: toward noble metal-free electro-catalysis, J. Mater. Chem. A 7 (2019) 11241-11249.

[18] D. A. Islam, K. Barman, S. Jasimuddin, H. Acharya, Synthesis of ultrasmall and monodisperse sulfur nanoparticle intercalated CoAl layered double hydroxide and its electro-catalytic water oxidation reaction at neutral pH, Nanoscale 11 (2019) 7560-7566.

[19] A. A. Lobinsky, V. P. Tolstoy, Synthesis of CoAl-LDH nanosheets and N-doped graphene nanocomposite via Successive Ionic Layer Deposition method and study of their electrocatalytic properties for hydrogen evolution in alkaline media, J. Solid State Chem. 270 (2019) 156-161.

[20] S. Kumar, G. Saeed, L. Zhu, K. N.Hui, N. H. Kim, J. H.Lee, 0D to 3D carbon-based networks combined with pseudocapacitive electrode material for high energy density supercapacitor: A review, Chem. Eng. J. (2020)126352.

[21] Q. Lin, J. N.Harb, Implementation of a thick-film composite Li-ion microcathode using carbon nanotubes as the conductive filler, J. Electrochem. Soc. 151 (2004) A1115.

[22] K. Sheem, Y. H. Lee, H. S. Lim, High-density positive electrodes containing carbon nanotubes for use in Li-ion cells, J. Power Sources 158 (2006) 1425-1430.

[23] F. Bonaccorso, L. Colombo, G. Yu, M. Stoller, V. Tozzini, A. C. Ferrari, R. S. Ruoff, V. Pellegrini, Graphene, related two-dimensional crystals, and hybrid systems for energy conversion and storage, Science, 347 (2015) 1246501.

[24] X. Wang, M. Lou, X. Yuan, W. Dong, C. Dong, H. Bi, F. Huang, Nitrogen and oxygen dual-doped carbon nanohorn for electrochemical capacitors, Carbon 118 (2017) 511-516.

[25] K. Murata, A. Hashimoto, M. Yudasaka, D. Kasuya, K. Kaneko, S. Iijima, The Use of Charge Transfer to Enhance the Methane-Storage Capacity of Single-Walled, Nanostructured Carbon, Adv. Mater. 16 (2004) 1520-1522.

[26] S. Zhu, L. Fan, X. Liu, L. Shi, H. Li, S. Han, G. Xu, Determination of concentrated hydrogen peroxide at single-walled carbon nanohorn paste electrode, Electrochem. Commun. 10 (2008) 695-698.

[27] X. Bian, Q. Fu, C. Qiu, X. Bie, F. Du, Y. Wang, Y. Zhang, H. Qiu, G. Chen, Y. Wei, Carbon black and vapor grown carbon fibers binary conductive additive for the $Li_{1.18}Co_{0.15}Ni_{0.15}Mn_{0.52}O_2$ electrodes for Li-ion batteries, Mater. Chem. Phys. 156 (2015) 69-75.

[28] G. Kresse, D. Joubert, From ultrasoft pseudopotentials to the projector augmented-wave method, Phys. Rev.

B 59 (1999) 1758-1775.

[29] G. Kresse, J. Furthmüller, Efficient iterative schemes for ab initio total-energy calculations using a plane-wave basis set, Phys. Rev. B 54 (1996) 11169-11186.

[30] J. B. Han, J. Lu, M. Wei, Z. L. Wang, X. Duan, Heterogeneous ultrathin films fabricated by alternate assembly of exfoliated layered double hydroxides and polyanion, Chem. Commun. (2008) 5188-5190.

[31] G. Pan, X. X, J. Luo, F. Cao, Z. Yang, H. Fan, Preparation of CoAl layered double hydroxide nanoflake arrays and their high supercapacitance performance, Appl. Clay Sci. 102 (2014) 28-32.

[32] S. Bandow, F. Kokai, K. Takahashi, M. Yudasaka, L. C. Qin, S. Iijima, Interlayer spacing anomaly of single-wall carbon nanohorn aggregate, Chem. Phys. Lett. 321 (2000) 514-519.

[33] C. M. Yang, D. Kasuya, M. Yudasaka, S. Iijima, K. Kaneko, Microporosity Development of Single-Wall Carbon Nanohorn with Chemically Induced Coalescence of the Assembly Structure, J. Phys. Chem. B 2004 108 (2004) 17775-17782.

[34] R. Jiang, C. Cui, H. Ma, Using graphene nanosheets as a conductive additive to enhance the capacitive performance of α-MnO_2, Electrochim. Acta 104 (2013) 198-207.

[35] G. Fan, H. Wang, X. Xiang, F. Li, Co-Al mixed metal oxides/carbon nanotubes nanocomposite prepared via a precursor route and enhanced catalytic property, J. Solid State Chem. 197 (2013) 14-22.

[36] Y. Gogotsi, R. M. Penner, Energy Storage in Nanomaterials-Capacitive, Pseudocapacitive, or Battery-like?, ACS Nano 12 (2018) 2081-2083.

[37] Z. Zhu, L. Qu, Y. Guo, Y. Zeng, W. Sun, X. Huang, Electrochemical detection of dopamine on a Ni/Al layered double hydroxide modified carbon ionic liquid electrode, Sens. Actuators B 151 (2010) 146-152.

[38] W. Lu, J. Shen, P. Zhang, Y. Zhong, Y. Hu, X. W. Lou, Construction of CoO/Co-Cu-S Hierarchical Tubular Heterostructures for Hybrid Supercapacitors, Angew. Chem., Int. Ed. 58 (2019) 15441-15447.

[39] H. S. Kim, J. B. Cook, H. Lin, J. S. Ko, S. H. Tolbert, V. Ozolins, B. Dunn, Oxygen vacancies enhance pseudocapacitive charge storage properties of MoO_{3-x}, Nat. Mater. 16 (2017) 454-460.

[40] V. Augustyn, P. Simon, B. Dunn, Pseudocapacitive oxide materials for high-rate electrochemical energy storage, Energy Environ. Sci. 7 (2014) 1597-1614.

[41] H.S. Kim, J. B. Cook, H. Lin, Jesse S. Ko, Sarah H. Tolbert, V. Ozolins, B. Dunn, Oxygen vacancies enhance pseudocapacitive charge storage properties of MoO_{3-x}, Nat. Mater. 16 (2017) 454-460.

[42] X. Li, J. Shen, W. Sun, X. Hong, R. Wang, X. Zhao, X. Yan, A super-high energy density asymmetric supercapacitor based on 3D core–shell structured NiCo-layered double hydroxide@carbon nanotube and activated polyaniline-derived carbon electrodes with commercial level mass loading, J. Mater. Chem. A 3 (2015) 13244-13253.

[43] L. Yu, N. Shi, Q. Liu, J. Wang, B. Yang, B. Wang, H. Yan, Y. Sun, X. Jing, Facile synthesis of exfoliated Co-Al LDH-carbon nanotube composites with high performance as supercapacitor electrodes, Phys. Chem. Chem. Phys. 16 (2014) 17936-17942.

[44] L. H. Su, X.G. Zhang, Y. Liu, Electrochemical performance of Co-Al layered double hydroxide nanosheets mixed with multiwall carbon nanotubes, J. Solid State Electrochem. 12 (2008) 1129-1134.

[45] X. Zhang, S. Wang, L. Xu, T. He, F. Lu, H. Li, J. Ye, Controllable synthesis of cross-linked CoAl-LDH/$NiCo_2S_4$ sheets for high performance asymmetric supercapacitors, Ceram. Int. 43 (2017) 14168-14175.

[46] Y. Zhang, D. Du, X. Li, H. Sun, L. Li, P. Bai, W. Xing, Q. Xue, Z. Yan, Electrostatic Self-Assembly of Sandwich-Like CoAl-LDH/Polypyrrole/Graphene Nanocomposites with Enhanced Capacitive Performance, ACS Appl. Mater. Interfaces 9 (2017) 31699-31709.

[47] T. Liang, H. Xuan, Y. Xu, J. Gao, X. Han, J. Yang, P. Han, D. Wang, Y. Du, Rational Assembly of CoAl-Layered Double Hydroxide on Reduced Graphene Oxide with Enhanced Electrochemical Performance for

Energy Storage, ChemElectroChem 5 (2018) 2424-2434.

[48] S. Wang, Z. Huang, R. Li, X. Zheng, F. Lu, T. He, Template-assisted synthesis of NiP@CoAl-LDH nanotube arrays with superior electrochemical performance for supercapacitors, Electrochim. Acta 204 (2016) 160-168.

[49] G. Wang, Y. Li, Z. Jin, "Ship in a Bottle" design of ZIF-9@CoAl LDH hybrid compound as a high performance asymmetric supercapacitor, New J. Chem. 44 (2020) 7528-7540.

[50] S. Sanati, Z. Rezvani, g-C_3N_4 nanosheet@CoAl-layered double hydroxide composites for electrochemical energy storage in supercapacitors, Chem. Eng. J. 362 (2019) 743-757.

[51] Y. Liu, C. Yu, H. Che, Z. Guo, J. Mu, X. Zhang, A. Liu, Ag nanoparticles-decorated CoAl-layered double hydroxide flower-like hollow microspheres for enhanced energy storage performance, J. Colloid Interface Sci. 581(2021) 485-495.

GRAPHICAL ABSTRACT

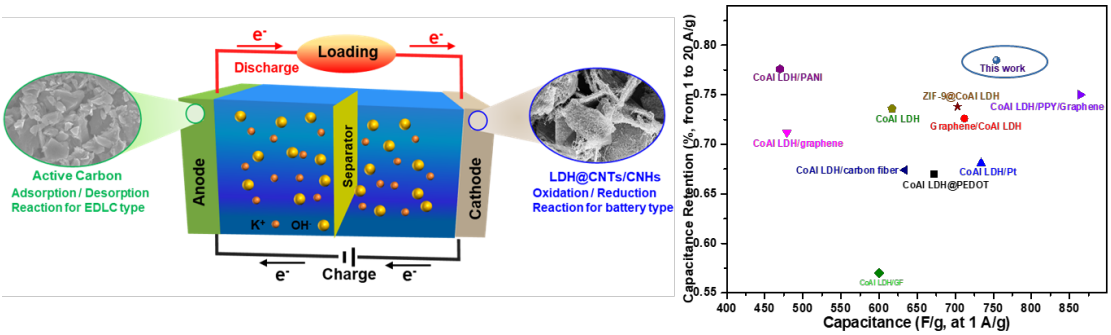

HIGHLIGHTS

- The CNTs/CNHs binary conductive additives design strategy is proposed.
- The CNTs/CNHs modified LDH electrode exhibits superior electrochemical performance.
- The synergistic mechanism between CNTs/CNHs and LDH are revealed.
- The LDH@CNTs/CNHs//Activated carbon hybrid supercapacitor are assembled.